Improved Detection of Lung Nodule Overlapping with Ribs by using Virtual Dual Energy Radiology

G.Maria Dhayana Latha

Associate Professor, Department of Electronics and Communication Engineering,

Excel Engineering College

Abstract- The main aim is to develop a CAD scheme with improved sensitivity and specificity by use of VDE CXRs where ribs and clavicles are suppressed with Massive Adaptive Training Artificial Neural Networks. To reduce rib-induced FPs and detect nodules overlapping with ribs, we incorporated the VDE technology in our CAD scheme. A nonlinear Super Vector Machine classifier was employed for classification of the nodule candidates. The average size of the nodules was 17.8 mm. 30% of the nodules were rated "extremely subtle" or "very subtle" by a radiologist. By using Virtual Dual Energy technology, more nodules overlapping with ribs or clavicles are detected and the sensitivity was improved substantially to 85.0% FP rate, whereas the FP rate was reduced to 2.5 per image. The sensitivity of our VDE-based CAD scheme for subtle nodules was higher than that of the original CAD scheme.

Index terms - Chest radiography (CXR), computer-aided diagnosis (CAD), lung cancer, rib suppression, virtual dual energy (VDE).False Positive (FP)

I. INTRODUCTION

In Cancer is a broad group of diseases involving unregulated cell growth. In cancer, cells divide and grow uncontrollably, forming malignant tumors, and invading nearby parts of the body. The cancer may also spread to more distant parts of the body through the lymphatic system or bloodstream. There are over 200 different types of known cancers that affect humans.

The causes of cancer are diverse, complex, and only partially understood. Approximately 5–10% of cancers can be traced directly to inherited genetic defects. Cancer can be detected in a number of ways, including the presence of certain signs and symptoms, screening tests, or medical imaging. Once a possibility of cancer is detected it is diagnosed by microscopic examination of a tissue sample.

Cancer is usually treated with chemotherapy, radiation therapy and surgery. The chances of surviving with the disease vary greatly by the type and location of the cancer and the extent of disease at the start of treatment. Currently, the overall five-year survival rate for lung cancer patients is only 14%. Early detection and treatment of lung cancers can improve the survival rate by 50% if the tumor is detected early at Stage 1, which is a solitary and circumscribed lung nodule. For detection of lung cancer at an early stage, computed tomography is a more sensitive imaging modality.

However, chest radiographs are used far more commonly for chest diseases because they are the most cost-effective, routinely available and dose-effective diagnostic tool. Because of CXRs are so widely used, improvements in the detection of lung nodules in CXRs could have a significant impact on early detection of lung cancer. However, 30% of nodules in CXRs were missed by radiologists in which nodules are visible in retrospect, and that 82–95% of the missed nodules is partly obscured by overlying bones such as ribs and clavicles. Such nodules would be more conspicuous on the soft-tissue images obtained by using the dual-energy subtraction technique

Therefore, a computer-aided detection scheme for nodules in CXRs has been investigated for assisting radiologists in improving their sensitivity. CAD schemes still produce a relatively large number of false positives. This will distract radiologists in their detection and reduce radiologists' efficiency. In addition, radiologists may lose their confidence with the CAD scheme has a high FP rate of 11 per images; radiologists' accuracy in detecting nodules is not improved when they are aided by computer output, even though the scheme has a high sensitivity of 80%. Radiologists' accuracy, however, it is significantly improved if the CAD scheme has a simulated low FP rate with the same sensitivity. Therefore, having a low FP rate is critical for a CAD scheme to be useful. A number of investigators developed FP reduction methods.

In spite of its great advantages, a limited number of hospitals use a dual-energy radiography system, because specialized equipment is required, and the radiation dose can be double.

To address the issue of the availability of dual-energy systems, Suzuki et al. developed an image-processing technique called virtual dual-energy (VDE) radiography for suppressing ribs and clavicles in CXRs by

means of a multi resolution MTANN. The real dual-energy images are used as the teaching images for training of the multi resolution MTANN. Once trained, real dual-energy images are not necessary any more.

II. METHODOLOGY

The lung nodules image is captured by using CXR, segmentation of lung nodules is done by using contra lateral subtraction method.
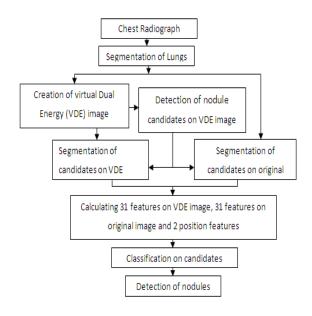

Fig 2.1 Block diagram of detection of lung nodules based on MTANNs

After segmentation lung nodules image ,VDE image is created for suppressing ribs and clavicles in CXRs by MTANN technique for separating soft tissue from bones in CXRs by use of two X-ray exposures at two different energy levels. Lung nodule detection on VDE is performed and segmentation on both original and VDE image is done to extract the feature on the both the image and based on the feature extraction classification is made and the nodules is detected on the lung.

2.1 MATERIALS AND METHOD

A)   Database of CXR: To train our CAD scheme, we collected 300 cases with nodules and 100 normal cases from six medical institutions by use of screen-film systems, computed radiography systems, and digital radiography systems. All nodules were confirmed by CT, and the locations of the nodules are confirmed by one of the chest radiologists. The nodule size ranged from 5 to 40 mm.

The poster anterior CXRs in the database are collected. All nodules in the CXRs are confirmed by CT, and the locations

of the nodules are   confirmed by three chest radiologists. Database is created a for evaluating VDE-based CAD scheme by excluding from the full JSRT database the nodules in the opaque portions of the CXR that correspond to the retro-cardiac and sub diaphragmatic regions of the lung, because the purpose of using the CAD scheme is to detect nodules in the lung fields.

B) Original Computerized Scheme for Nodule Detection: Our original CAD detection of lung nodules in CXRs consisted of four major steps:

Segmentation of lung fields based on our multi segment active shape model

Two-stage nodule enhancement and nodule candidate detection;

Segmentation of nodule candidates by use of our clustering watershed algorithm

Feature analysis and classification of the nodule candidates into nodules or non-nodules by use of a nonlinear SVM classifier.

Our MASM for lung segmenting is an improved model for the formulation on nodules by fixating selected nodes at specific structural boundaries called transitional landmarks. The transitional landmarks determined multiple segments, each of which corresponded to a specific boundary type such as the heart, aorta, and rib-cage. This allowed the nodes to learn local appearance models for a specific boundary type, rather than generalizing over multiple boundary types, which resulted in a marked improvement in boundary accuracy. After the lungs were segmented, a background-trend-correction technique based on the following second-order bivariate polynomial function was applied to the segmented lung field:

$F(x, y) = ax^2 + by^2 + cxy + dx + ey + f$ where *a, b, c, d, e*, and *f* are coefficients.

The two-stage nodule enhancement technique produced a nodule enhanced image and a nodule-likelihood map. The first stage of the technique enhanced nodules by use of two different types of gray-level morphologic opening operators: one enhanced nodules; the other suppressed ribs. The second stage of the nodule enhancement converted the nodule enhanced image into a nodule likelihood map by use of a directional gradient magnitude filter. Local peaks in the map were detected as nodule candidates.

To segment the nodule candidates, our "coarse-to-fine" segmentation technique based on morphologic filtering and improved watershed segmentation is employed. Binary morphologic erosion operator is applied to the nodule candidate regions to break connections between the nodule and non-nodule regions. Next, a binary morphologic dilation operator dilated the connected region. To refine the rough segmentation, developed a clustering watershed segmentation technique. Peaks within the rough nodule candidate region in the nodule-enhanced image are obtained. With the watershed segmentation, the rough nodule candidate region is divided into several catchment basins.

$$\{\ \overrightarrow{I}(x,y),T(x,y)\ x,y \in R_T\ \} =$$

$$(\overrightarrow{I}_1, T_1), (\overrightarrow{I}_2, T_2), \dots, (\overrightarrow{I}_N, T_N) \qquad (3.2\ )$$
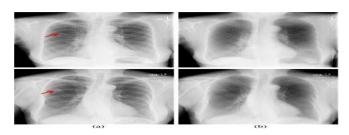

Fig 2.2 Ribs and clavicles were suppressed by using our MTANN technique. (a) Original CXR. (b) VDE soft-tissue image.

Each minimum point is surrounded by a catchment basin associated with it; thus, there are one or more peaks, each of which is surrounded by a cluster of connected pixels that constituted a catchment basin. From the multiple catchment basins, a single nodule candidate region is determined by clustering method: first, a primary cluster is defined as a cluster that contained the nodule candidate location determined by the initial nodule candidate detection step. Clusters connected to the primary cluster were added. The connected clusters are identified by use of the criterion that the minimum value between the peak in the primary cluster and each of the other peaks is larger than a threshold value.

2.2 STEP IN DETECTING LUNG NODULES

A)   Creation of VDE Images: An image processing technique for suppression of ribs and clavicles in CXRs has been developed by means of a multi resolution MTANN. With this technique, ribs and clavicles in CXRs can be suppressed substantially, while soft tissues such as lung nodules and vessels are maintained. Fig. 3.1 shows examples of VDE images in which ribs and clavicles are suppressed by use of the MTANN technique. MTANN is a highly nonlinear filter that can be trained by use of input CXRs and the corresponding "teaching" images. Bone images obtained by use of a dual-energy radiography system are used as the teaching images. The MTANN consisted of a linear-output ANN regression model that is capable of operating on image data directly. Single pixels corresponding to the centers of the input sub regions are extracted from the teaching images as teaching values, represented by

$$f(x,y) = NN(\overrightarrow{I}\ x,y) \qquad (3.1\ )$$

here $\overrightarrow{I}\ x,y,\ = \{g\ (x-i, y-j)\ |\ I, j \in R$

is the input vector to the MTANN which is a subregion extracted from CXR, and $f(x, y)$ is an estimate for a teaching value. The MTANN is massively trained by using each of a large number of the input subregions together with each of the corresponding teaching single pixels. The training set of pairs of a subregion and a teaching pixel is represented by

where $T(x, y)$ is a teaching image, R_T is a training region which corresponds to the collection of the centers of sub region, and N_T is the number of pixels in R_T .

For a single MTANN, suppression of ribs containing various frequencies was difficult, because of the capability of a single MTANN was limited. First, a lower resolution image $g_L(x,y)$ was obtained from an original higher resolution image $g_H(x,y)$ by performing down sampling with averaging, i.e., four pixels in the original image are replaced by a pixel having the mean value for the four pixel values, represented by

$$\frac{1}{4} \sum_{i,j \in R22} gH(2x - i, 2y - j) \qquad (3.3)$$

where R_{22} is a 2×2 pixel region. i.e., a pixel in the lower resolution image is replaced by four pixels with the same pixel value, as follows:

$$gLU(x,y) = \left(gL\left(\frac{x}{2}, \frac{y}{2}\right) \right) \qquad (3.4)$$

Then, a higher resolution difference image $d_H(x,y)$ is obtained by subtraction of the enlarged lower resolution image from the higher resolution image, represented by

$$dH(x,y) = gH(x,y) - gLU(x,y) \qquad (3.5)$$

These procedures are performed repeatedly, producing further lower resolution images. An important property of this technique is that exactly the same original resolution image $g_H(x,y)$ can be obtained from the multi resolution images, as follows:

$$gH(x,y) = gLU(x,y) + dH(x,y) \qquad (3.6.)$$

For suppression of ribs and clavicles in an original CXR $g(x, y)$, a VDE image $f_b(x, y)$ produced by the trained multi resolution image $m(x, y)$ as follows:

$$fs(x, y) = g(x, y) - wc * fb(x, y) * m(x, y) \qquad (3$$

where w_c is a weighting parameter for determining the contrast of ribs. By changing the weighting parameter w_c.

B) CAD Scheme Combined With VDE Technique:

CAD scheme combined with the VDE technology for detection of lung nodules in CXRs. To reduce rib-induced FPs and detect nodules overlapping ribs and clavicles, we incorporated the VDE technology in CAD scheme. The VDE-based CAD scheme detected nodule candidates on VDE images by use of the two-stage nodule enhancement technique applied in our original CAD scheme. In the VDE-based CAD scheme detected nodule candidates on VDE images by use of the two stage nodule enhancement technique. A watershed segmentation algorithm is employed to segment each candidate in both original and VDE CXRs.
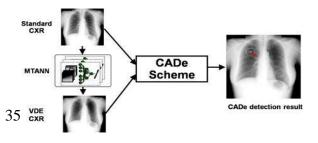
Fig 2.3 Our CAD scheme for detection of lung nodules in CXRS by use of our VDE technology based on MTANNs
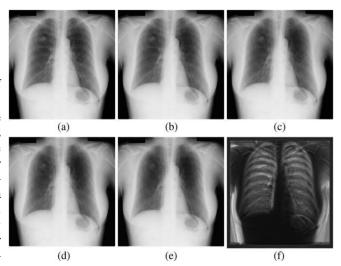
Sixty morphologic and gray-level-based features are extracted from each candidate from both original and VDE CXRs which are smaller than the number of nodules in the training database. A nonlinear SVM is employed for classification of the nodule candidates into nodules or non-nodules. In our CAD scheme, only CXR acquired with a standard radiography system was inputted into our system and no specialized equipment for generating VDE image, but only software, is required. A nonlinear SVM is employed for classification of the nodule candidates into nodules or non-nodules.

Major challenges for original CAD scheme are to detect the nodules overlapped with ribs, rib crossings, and clavicles, and reduce the FPs caused by these structures. Because of the rib and clavicle suppression in VDE images, nodules are more obvious than those in the original images.

The detected nodule candidates in VDE images are to improve the sensitivity for detection of nodule candidates. It looks forward to reduce most of the FPs that is caused by these structures by the incorporation of VDE image in the nodule candidate detection. Some nodules have similar characteristics those of bones in terms of the shape, the size, the contrast, and the orientation. The features of nodules may be suppressed in VDE image.To improve the classification performance, it also extracted the same feature set at the corresponding locations of the detected nodule candidates in the corresponding original image. Nodule candidate segmentation was repeated both in original and VDE images.

To determine the performance of the VDE-based CAD scheme, this incorporated the VDE technique. We first defined how to train the MTANN to create the VDE images for the CAD scheme. Next, the sensitivity for nodules candidate detection on VDE images with different rib contrast is presented and compared to that on the original image. The

overall system performance is quantified using FROC curves. The SVM classifier and linear discrimination analysis (LDA) classifier are trained/tested with a leave-one-out cross-validation test. In our CAD schemes, all features are extracted and selected for each CAD scheme are given in Table 2.1.

Table 2.1 Features selected for three CAD schemes by use of the feature selection method

From the table, we can see that the number of selected features for VDE image is equal to that for original image. However, there are some different features selected and more density-based features instead of nodule-rib image-based features are selected for VDE image.

C) TRAING METHODS: We used four CXRs and their corresponding dual-energy bone images in a training set for training the multi resolution MTANN. One of the major advantages of the MTANN technique is that it only needs a few number of dual-energy training images. In the four cases, one is a normal case and the other three contained with nodules.

Fig 2.4 Illustration of changes in rib contrast in VDE soft-tissue images and the VDE bone.

D) Nodule Candidate Detection: Fig 2.4 shows that the VDE bone image and the VDE soft tissue images with difference rib contrast processed by multi resolution MTANN technique.
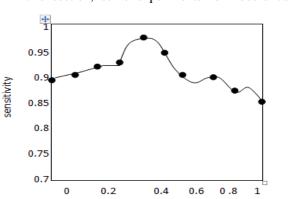
The training samples for the nodules are extracted by manual in order to make it cover the nodule. The size of the sub region for MTANNs is 9×9 pixels. It is sufficient to cover the width of rib in the resolution image. Three-layered MTANNs are used in experiments where the numbers of input, hidden, and output units are 81, 20, and 1, respectively.

In this section, some experiments for nodule candidate detection based on the VDE

Extracted features	Original CXRs	VDE CXRs	VDE and Original CXRs
Can .X	*	#	#
Can .y	*		#
Can .Grad$_1$			
Can .Cv$_1$	*	#	
Can .Grad$_2$			
Can .Cv$_2$		#	*,#
Shape$_1$		#	*
Shape$_2$			#
Shape$_3$			
Shape$_4$	*		*
Gray$_1$			*
Gray$_2$		#	
Gray$_3$	*		
Gray$_4$	*		#
Gray$_5$	*		*
Grad$_1$	*	#	
Grad$_2$	*		
Grad$_3$	*	#	*,#
Surface$_1$		#	*
Surface$_2$			
Surface$_3$		#	
Texture$_1$		#	
Texture$_2$			
Texture$_3$			
Texture$_4$			
FP			#

images are conducted. The "region" criterion is adopted to determine a true positive (TP) which is also applied in the original CAD scheme. Image used to create those soft-tissue images. (a) Original image. (b) VDE soft-tissue image with 20% rib contrast. (c) 40% rib contrast. (d) 70% rib contrast. (e) 90% rib contrast. (f) VDE bone image.

The "bone-like-image" is subtracted from the original CXR to get the VDE soft tissue image. The parameter m_c to adjust the rib contrast in VDE image. Different parameters can have an influence on the nodule candidate detection performance.

Fig 2.5 Effect of the change in rib contrast on the sensitivity of our CAD scheme.

Fig. 2.5 shows the performance of the nodule candidate detection stage with different rib contrast. The sensitivity is highest when the rib contrast parameter m_c is set 0.4. The most nodules are detected in the nodule candidate detection step and the contrast of nodule is more obvious for the CAD scheme.

In this experiment, 70 candidates that have max code values in the nodule are likelihood map are selected for each image. If the distance between any two peaks is less than 5 mm, then a candidate is created only from the peak with the highest value. The nodule candidate detection stage in the VDE-based CAD scheme achieved a sensitivity of 96.4% (135/140) with 70 candidates per image. The missed nodules in the candidate detection step from original CXR, but detected from VDE image

E) Performance of the Scheme Only Using VDE Image
: The VDE image is applied to replace the original image in the original CAD scheme. The nodule candidates are detected from the VDE image by use of the two-stage nodule enhancement method. Then, 31 features are extracted from the VDE image after nodule candidate segmentation. The performance of the CAD scheme only using VDE image is higher than that of original CAD scheme , i.e., it achieved a sensitivity of 65.7% (92/140) by use of VDE image and a sensitivity of 60.7% (85/140) by use of original image at an FP rate of 1.5 FPs per image for nodule cases. The CAD scheme only using VDE image detected 12 more nodules, which are missed by the CAD scheme using original image at 5 FPs per image on average.

Most of these nodules are very subtle or extremely subtle nodules in the JSRT database. However, five nodules are missed by the CAD scheme using VDE image, while they are detected by the original CAD scheme and they are non subtle nodules. So there is only 5% improvement with 5 FPs per image. It is interesting to note that the sensitivity of CAD scheme only using original image is higher than that of CAD scheme only using VDE image at a lower FP rate. The reason is that the contrast of some nodules in VDE images is improved because of the rib suppression and it is visible for our CAD scheme to detect them.

Based on this phenomenon, we also segmented the candidates and extracted the features from the original image at the same location which are detected in the VDE image.

Rib edges are segmented as the nodule boundaries, but classified as TP by use of the features based on both original and VDE image. But some nodules are smoothed when using the MTANN technique to suppress the ribs in CXR
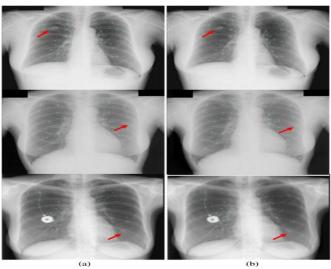

Fig 2.6 Improvement in detection of nodule candidates by use of our VDE technology. (a) Nodule candidate detection results based on original images.(b) Nodule candidate detection results based on VDE images.
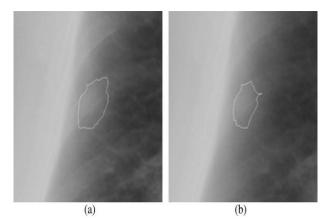

Fig 2.7 Illustration of the nodules detected in the nodule candidate detection step (a) Nodules with segmentation results in original image. (b) Nodules with segmentation results in VDE images.

Fig. 2.7 illustrates that the nodule detected in the nodule candidate detection step is classified as FP by use of the features based on original image because some rib edges are segmented as the nodule boundaries.

The CAD scheme only using VDE image detected 12 more nodules, which are missed by the CAD scheme using original image at 5 FPs per image on average
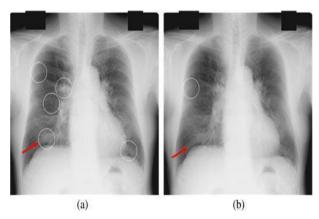
Fig 3.8 Illustration of detection of nodules   (a) TP and FPs of the original CAD scheme. b) FN and FP of the VDE-based CAD scheme.

The detection of lung nodules provide efficient method to detect the nodules which are   suppressed in ribs and clavicles in the lung with the help of VDE based CAD scheme provide TP and FP in the original CAD scheme as well as in VDE based CAD scheme.

F) Performance of Scheme Using VDE Combined With Original Image: FROC curves showing the overall performances of the VDE-based CAD scheme, which combined VDE image with original image, and the original CAD scheme for the JSRT in a leave-one-out cross-validation test with SVM.

The performance of the VDE-based CAD scheme is substantially higher than that of the original CAD scheme, i.e., the VDE-based CAD scheme achieved a sensitivity of 85.0% (119/140) and the original CAD scheme achieved a sensitivity of 78.5% (110/140) at an FP rate of 5.0 FPs per image for the JSRT database. In the VDE-based CAD scheme, 11 nodules were detected while they are missed in the original CAD scheme and only two nodules) were missed
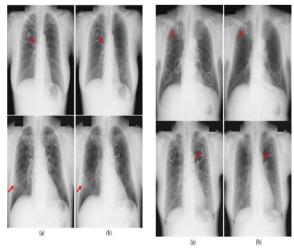

Fig 2.9 Illustration of the improvement in nodule detection with our VDE technology. CAD marks are indicated by circles. (a) False negatives (arrow) and FPs of the original CAD scheme. (b) TPs (arrow) and FPs of the VDE-based CAD scheme with the VDE technology

We analyzed the CAD scheme performance according to nodule subtlety, size, and pathology, as shown in Figs. 10–12 for the JSRT database. The sensitivity is calculated in each category. The VDE-based CAD scheme marked 66.7% (28/42) of very subtle and extremely subtle nodules with 5 FPs per image. All obvious nodules are marked with 2.5 FPs per image, and 92.1% (35/38) of relatively obvious nodules are detected with 1.6 FPs per image.

It is more visible to detect the lung node. The VDE-based CAD scheme has a high performance with a sensitivity of 87.1% (54/62) with 5.0 FPs per image for the medium-sized nodules and a relatively high performance with a sensitivity of 79.3 % for small nodules. The sensitivities for malignant and benign nodules are moderate. The VDE-based CAD scheme detected the truth nodules with few FPs, whereas the original CAD scheme missed the truth nodules, and most of the FPs is located in the ribs, rib intersections, and the clavicles.

Fig.2.10 shows two examples that the FPs which is detected in the original scheme is reduced in the VDE-based CAD scheme. The VDE-based CAD scheme not only can detect more nodules which are overlapped with ribs or clavicles, but also can reduce the FPs deduced by the ribs and clavicle. Thus, the overall performance is substantially improved by use of the VDE technique.

The main reason is that these nodules have characteristics similar to those of ribs in terms of the shape, the size, the contrast, the orientation, the texture, and the margin. Another reason is that, in the experiment, the images are scanned from films. MTANN that is used to create the VDE image is trained by four cases, which are obtained from a dual-energy CR system. The rib contrast and resolution in the digital radiograph are higher than that scanned from films.
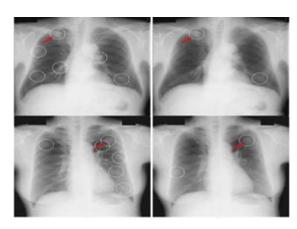

Fig 2.10 Illustration of the improvement in specificity by our VDE technology. (a) TPs and FPs of the original CAD scheme. (b) TPs and FPs of the VDE-based CAD scheme.

3.4.5 Performance Comparison with Others
It is difficult to make definitive comparisons with previous CAD schemes because of different databases, different TP

criteria, different evaluation procedures, different optimization parameters, and different operating points. The result found four studies in which the publicly available JSRT database is used. It particularly difficult to detect the very small and extremely subtle nodules in the JSRT database and the radiologist detected only 44% of the hard cases. With an average 4 FPs per image, our VDE-based scheme correctly marked 66.7% of the hard cases. There is 10% improvement than the original scheme, and it also have a higher performance than other.

Table 2.2 summarizes the performance comparisons among different CAD schemes in the literature. Wei *et al*. reported that their CAD scheme achieved a sensitivity of 80% with 5.4 FPs per image for the JSRT database.

Table 2.2 Performance comparisons of CAD schemes that used the JSRT database for evaluation in the Literature

	Sensitivity	FP/image	Database
Wei et al.(2002)	80%(123/154)	5.4(1333/247)	All nodule and normal cases in JSRT(247)
Coppini et al.(2003)	60%(93/154	4.3(662/154)	All nodule cases in JSRT(154)
Schiham et al.(2006)	51%(79/154) 67%(103/154)	2.0(308/154) 4.0(616/154)	All
Hardie et al.(2009)	80%(112/140) 63%(88/140)	5.0(700/140) 2.0(280/140)	Nodule cases in JSRT(140)
Chen et al.(2011)	79%(110/140) 71%(100/140)	5.0(1165/233) 2.0(466/233)	Nodule cases and all normal cases in JSRT(233)
VDE based CAD	85%(119/140)	5.0(1165/233)	Nodule cases and all normal cases in JSRT(233)

Their performance is calculated by use of the "distance" criterion of 25 mm for determining TP detections. The VDE-based CAD scheme achieved a sensitivity of 85.0% (119/140) and 77.9% (109/140); CAD scheme achieved a sensitivity of 80.0% and 63% at FP rates of 5.0 and 2.0 per image, respectively.

III. CONCLUSION AND FUTURE WORK

The method is aimed at the development of a model to an efficient method for development of computerized scheme for detection of lung nodules by incorporating VDE image in which ribs and clavicles were suppressed by an MTANN technique.

The future enhancement will be develop a efficient system that provide efficient with improvement in increasing VDE in

CXR and to reduce the result of FP rate , also to increase sensitivity.

IV. REFERENCES

[1] Carlos S. Pereira, Luıs A. Alexandre, Ana Maria Mendona,and Aurelio campiho,(2006) "A Multi classifier Approach for Lung Nodule Classification" pp.612–623.

[2] S. Chen, K. Suzuki, and H. MacMahon, (2011) "Development and evaluation of a computer-aided diagnostic scheme for lung nodule detection in chest radiographs by means of two-stage nodule enhancement," Med.Phys., vol. 38, pp. 1844–1858.

[3] Elaheh , Soleymanpour, Emad Ansaripour1, (2011) " Fully Automatic Lung Segmentation and Rib Suppression Methods to Improve Nodule Detection in Chest Radiographs", Journal of Medical Signals & Sensors, Vol 1.No .3.

[4] R. Engelmann, F. Li, K. Doi, and H. MacMahon, (2008) "Improved detection of small lung cancers with dual-energy subtraction chest radiography,"AJR Amer. J Roentgenol., vol. 190, pp. 886–891.

[5] R. C. Hardie , S. K. Rogers, T. Wilson, and A. Rogers, (2008) "Performance anal-ysis of a new computer aided detection system for identifying lung nodules on chest radiographs". Jun

[6] Hui Zhaoa, b, Shih-Chung Ben Loa, Matthew T. Freedmana, and Yue Wangb (2007) "Enhanced Lung Cancer Detection in Temporal Subtraction Chest Radiography Using Directional Edge Filtering Techniques", a ISIS Center.

[7] M. Loog, B. van Ginneken, and A. M. Schilham, (2006) "Filter learning: Application to suppression of bony structures from chest radiographs," Med. Image Anal., vol. 10, pp. 826–840.

[8] A. M. Schilham, B. van Ginneken, and M. Loog, (2006) "A computer-aided diagnosis system for detection of lung nodules in chest radiographs with an evaluation on a public database," Med. Image Anal., vol. 10, pp. 247–258.

[9] Shang Chen and Kenji Suzuki, (2013) "Computerized Detection of Lung Nodules by Means of -Virtual Dual-Energy Radiography", IEEE transactions on biomedical engineering, vol. 60, no. 2.

[10] K. Suzuki, H. Abe, H. MacMahon, and K. Doi, (2006) "Image-processing tech-nique for suppressing ribs in chest radiographs by means of massive training artificial neural network (MTANN)," IEEE Trans. Med. Imag., vol. 25, no. 4, pp. 406–416.

[11] K. Suzuki, J. Shiraishi, H. Abe, H. MacMahon, and K. Doi,(2005) "False-positive reduction in computer-aided diagnostic scheme for detecting nodules in chest radiographs by means of massive training artificial neural network," Acad. Radiol., vol. 12, pp. 191–201.